Hindawi
Advances in Civil Engineering
Volume 2018, Article ID 8978467, 12 pages
https://doi.org/10.1155/2018/8978467

Research Article

Effects of Burial Depth on the Seismic Response of Subway Station Structure Embedded in Saturated Soft Soil

Xuelei Cheng and Zongguang Sun

Transportation Engineering College, Dalian Maritime University, Dalian, Liaoning 116026, China

Correspondence should be addressed to Xuelei Cheng; xueleic@163.com

Received 28 May 2018; Accepted 16 August 2018; Published 5 September 2018

Academic Editor: Antonio Formisano

For the aim to study the effects of burial depth on seismic response in the subway station's structure embedded in saturated soft soil, on the basis of the OpenSEES program, numerical models with four cases of burial depth for the nonlinear interaction system including subway station's structure and saturated soft soil are developed with the *u-p* formulations of Biot's theory as it seeks to describe the saturated two-phase media. The effects of burial depth on the seismic response and the failure pattern of the subway station structure are investigated. The numerical results show that (1) the burial depth has a significant effect on the nonuniform uplift of station's structure due to the movement of soil from far field towards baseplate; (2) with the increase of burial depth, the inertial effect of overlaying soil of the subway station structure becomes more obvious, and the peak zone of the pore pressure ratio contracts from the outer area to the baseplate bottom with decreasing amplitude; (3) the dynamic index R decreases with the increasing burial depth of the station's structure; and (4) in terms of the middle column, the burial depth of the station's structure has the most crucial effect on the additional dynamic shear force and bending moment at the top end.

1. Introduction

The current antiseismic code design of the subway station structure system in the soft soil site is rougher than that of liquefiable sandy soil foundation. There are only a number of qualitative and general provisions, and there is still a lack of more in-depth and systematic research [1–4]. In this way, the consideration of the influence of the soft site on seismic response of the subway station structure dynamic system has an important theoretical value and practical significance to deepen the antiseismic understanding of the subway station structure and promotes the development of geotechnical earthquake engineering. As we all know, burial depth is one of the important factors that affect the seismic response of subway station structures [5, 6]. All previous earthquake disasters show that the subway station structure with a different thickness of a soft overlying soil layer has different site effects; that is, the dynamic damage degree and model of the subway station structure in the saturated soft soil site under different burial depth conditions has a significant difference [7, 8]. On the one hand, the shear effect and the soil dynamic pressure of the overlaying soil layer on the subway station structure are increased with the increase of the burial depth, which is unfavorable to the seismic response of the subway station structure. On the other hand, the constraint effect of the site on the subway station structure is strengthened with the increase of the burial depth, restricting the deformation reaction of the subway station structure, which is beneficial to the seismic response of the subway station structure. Therefore, it is significantly necessary and urgent to study the seismic response characteristics of subway stations under different burial depth conditions in the soft site.

Many scholars have conducted many researches on the seismic response of the subway station structure under different burial depth conditions. Liu et al. [9, 10] applied the nonlinear liquid-solid two-phase body dynamic finite element method to study the response of the burial depth of the subway station structure in the saturated liquefiable sand site under the horizontal and vertical seismic actions. Bilotta et al. [11] based on the total stress finite element method studied the dynamic response of a circular tunnel of 6 m diameter, with the axis at a depth of 15 m in a 30 m thick

layer of medium dense gravel, sand, or soft clay, overlying a relatively stiff bedrock. Chen et al. [12] studied the response of the burial depth to the seismic displacement of the subway station structure based on the dynamic total stress finite element method and compared and analyzed the internal forces of the subway station structure under the seismic action. Zhuang et al. [13] made numerical simulation analysis of the seismic response of the subway station structure in 5 soft sites of the two-storey three-span island subway station with soft soil layers of different burial depth conditions in the side and bottom foundations and 1 general site based on the dynamic total stress finite element method. Amorosi et al. [14] adopted two different approaches, both accessible in the engineering practice to evaluate the increments of seismic-induced loads in the transverse direction of the tunnel lining in terms of hoop force and bending moment to study the seismic transversal response of a shallow tunnel built in two ideal clayey deposits of different consistencies. Chen et al. [15] based on the dynamic total stress finite element method carried out the numerical analysis of rock mass and tunnel lining and modeled the incident waves as harmonic S and P waves to investigate the influence of the depth of a tunnel on its seismic damage. Wang et al. [16] used the ultimate shear stress as the failure criterion based on the dynamic total stress finite element method, simulated the seismic damage process of the subway station structure by the birth-death element method, and considered the impact of the initial ground stress on the antiseismic property of the subway station structure by the burial depth of the structure. Li et al. [17] established two analysis models of subway station structure' burial depth based on the dynamic total stress finite element method to study the influence of the distribution of different soil layers of layered foundation on the seismic response of the structure. Tsinidis [18] conducted a numerical parametric study on diverse soil-rectangular tunnel systems, aiming at shedding light on critical response characteristics of rectangular tunnels subjected to transversal ground shaking based on the dynamic total stress finite element method. Cui et al. [19] adopted the orthogonal design scheme of the "four factors and three levels" numerical test and two-phase medium dynamic analysis method to analyze the dynamic response characteristics and the catastrophic mechanism of the subway station structure in the soft site and combined with the multiindex comprehensive balance method to carry out the sensitivity analysis of material parameters in view of the changes of the indexes such as the dynamic pore pressure ratio at the soil typical point and the dynamic response indexes including the internal force at the characteristic positions of the subway station structure caused by the change of soft foundation soil parameter factors.

Due to the complexity of the research problem of the antiseismic subway station structure in the saturated soft soil site and the limitation of calculation theory and hardware calculation, most of the existing research results in the subject of the seismic response of the subway station structure under the conditions of different burial depth conditions in the soft soil site are based on the total stress dynamic analysis method without considering the influence of pore pressure, in which the influence of dynamic pore pressure distribution change cannot be considered [20]. However, the decoupled effective stress dynamic analysis method based on the pore pressure model has some limitations in the complex stress state deformation characteristics of saturated soil [21, 22]. It is rare in the existing research results to comprehensively consider the complex factors such as the multiphase medium property of saturated soft soil, the dynamic nonlinearity of the foundation-structure system, and so on to conduct the related research on the effect of burial depth on the underground structure.

On this base and based on the characteristics and limitations of the existing domestic and foreign research results, the dynamic Biot' two-phase medium coupling theory is adopted to describe the dynamic constitutive nonlinearity of saturated soft soil with the elastoplastic multiyield surface plastic kinematic model, and the nonlinearity dynamic performance of the station structure is described with the fiber section element and the modified Kent–Park concrete model. On this basis, the effective stress coupling nonlinear dynamic numerical solving model is established to analyze the effect of burial depth on the seismic response of the subway station structure dynamic system in the saturated soft soil layer, so as to provide guidance and reference for the antiseismic design and analysis of the subway station structure in the soft soil site.

2. Numerical Calculation Model

The numerical example is based on the typical single-storey double-span subway station in the saturated soft clay site, as shown in Figure 1, in which the cross section size of the subway station structure is 17 m (width), 7.17 m (height), and 3.5 m (center column spacing). Figure 2 shows the 2-dimensional plane strain finite element model mesh of the established dynamic system of the subway station structure in saturated soft soil foundation, the size of which is 170 m × 30 m. The more unfavorable cases between soil and structure of complete bond and coordinated deformation are considered without considering the separation and sliding between them. Four different burial depth working conditions (2 m, 5 m, 8 m, and 11 m, resp.) are established to make a related analysis of the coupled effective stress numerical model for the saturated soft soil site-subway station structure dynamic interaction system.

In the analyses, the boundary between the soil deposit and the bedrock was assumed fixed in both horizontal and vertical directions and serving as the bottom boundary of the analyzed domain. The ground surface was assumed flat and free of loadings. The test simulated the free-field boundary conditions using laminar boxes. In the OpenSEES program, the behavior of the laminar box can be modeled by adopting the tied node feature. This feature allows the horizontal and vertical displacements at the two boundaries with the identical value. The stress-strain behavior of the material model for saturated soil could simulate the hysteresis damping to a certain extent. The bottom and both sides of the site are set as undrained boundaries, the surface is set as

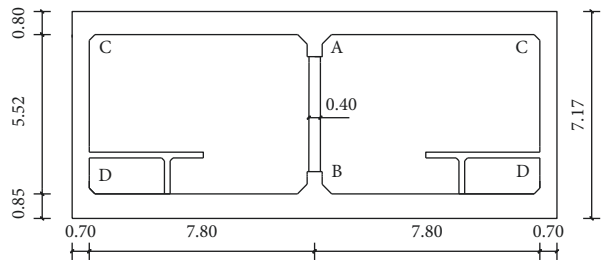

Figure 1: The cross section of the subway station structure (unit: m).

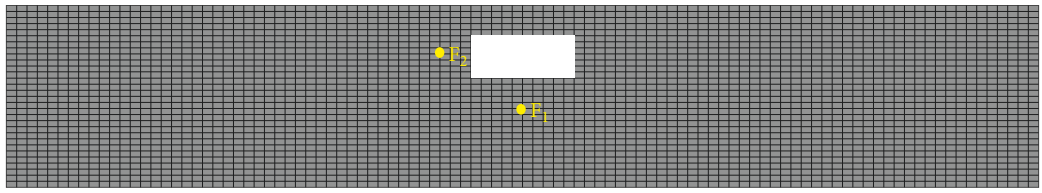

Figure 2: Finite element model of calculation.

a drainage boundary, and both sides of the model are set as the tied boundary [23]. The more unfavorable cases are considered without considering the separation and sliding between soil and structure, that is, complete bond and coordinated deformation between them [24, 25]. Energy dissipation effect is stimulated by the Rayleigh damping adopted in the numerical model, and the specific damping ratio is selected as 5% [26]. The HHT step-wise time integration method is used in the dynamic calculation, which can consider the energy dissipation and the second-order accuracy.

The numerical formula of the saturated two-phase medium matrix used in the present paper is as follows [27]:

$$\begin{aligned} \mathbf{M}\ddot{\mathbf{u}} + \mathbf{C}\dot{\mathbf{u}} + \int_{\Omega} \mathbf{B}^{T}\boldsymbol{\sigma}' d\Omega - \mathbf{Q}\mathbf{p} &= \mathbf{f}^{u}, \\ \mathbf{Q}^{T}\dot{\mathbf{u}} - \mathbf{S}\dot{\mathbf{p}} - \mathbf{H}\dot{\mathbf{p}} &= \mathbf{f}^{p}, \end{aligned} \tag{1}$$

where $\mathbf{M}$ is the total mass matrix; $\mathbf{u}$ is the displacement vector; $\mathbf{B}$ is the strain-displacement matrix, $\mathbf{B} \equiv \mathbf{L}\mathbf{N}^{u}$, which is related to the strain and displacement increment $d\boldsymbol{\varepsilon} = \mathbf{B}\overline{du}$; $\boldsymbol{\sigma}'$ is the effective stress tensor; $\mathbf{Q}$ is the discrete gradient operator for soil-water coupling; $\mathbf{p}$ is the pore pressure vector; $\mathbf{S}$ is the compression coefficient matrix; $\mathbf{H}$ is the permeability coefficient matrix; and vectors $\mathbf{f}^{\mathrm{u}}$ and $\mathbf{f}^{\mathrm{p}}$, respectively, indicate the given boundary conditions of the volume force in the soil-water mixture and the liquid phase.

The u-p form plastic constitutive relation of the elastic-plastic multiyield surface motion based on Biot's theory as shown in Figure 3 is adopted for clay. The yield surface formula of the clay multiyield surface model is

$$\begin{aligned} \mathbf{f}_{m} &= \left\{\frac{3}{2}\left(\tau - \alpha^{(m)}\right) : \left(\tau - \alpha^{(m)}\right)\right\}^{1/2} \\ &- \mathbf{K}^{(m)} = 0 \\ &(m = 1, 2, \ldots, n), \end{aligned} \tag{2}$$

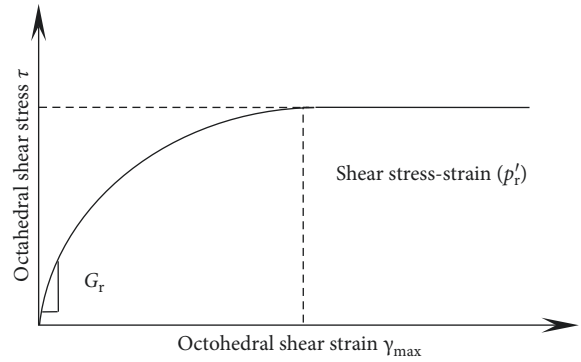

Figure 3: Shear stress-strain curve of soft soil.

where τ is the partial stress tensor; m is the number of the mth yield surface, $m \in (1, 2, \ldots, n)$; n is the total quantity of the yield surface; the parameters $\alpha^{(m)}$and $\mathbf{K}$, respectively, indicate the center and radius of the mth yield surface; and $\mathbf{K}^{(m)}$ is equal to $\sqrt{3/2}$times of the radius of the yield surface. The double dot product of tensors $\mathbf{A}$ and $\mathbf{B}$ is $\mathbf{A} : \mathbf{B} = \mathbf{A}_{ij} : \mathbf{B}_{ij}$.

The plastic constitution of the clay multiyield surface adopts the law of partial kinematic hardening, and the movement direction tensor of the yield surface is defined as

$$\mu = \left[\mathbf{s}_{\mathrm{T}} - \alpha^{m}\right] - \frac{\mathbf{M}_{m}}{\mathbf{M}_{m+1}}\left[\mathbf{s}_{\mathrm{T}} - \alpha^{m+1}\right], \tag{3}$$

where $\mathbf{s}_{\mathrm{T}}$ is the second-order deviatoric stress tensor, which represents the deviatoric stress tensor of the intersection point of the yield surfaces $\mathbf{f}_{m+1}$ and $\mathbf{f}_{m}$, and $\alpha_{m}$and $(p' + p'_{0})\alpha_{m+1}$are the center of the yield surfaces $\mathbf{f}_{m}$ and $\mathbf{f}_{m+1}$, respectively.

Figure 4 shows a representation of the nonlinear soil behavior in terms of normalized shear modulus and damping curves vs shear strain amplitude and a comparison

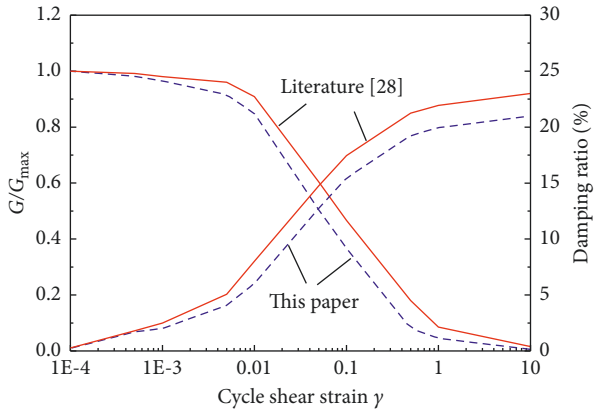

Figure 4: Comparison of the $(G)/(G)_{max}$ vs γ and λ vs γ curves.

with standard literature behaviors [28]. It can be seen that the nonlinear soil behavior in terms of normalized shear modulus and damping curves vs shear strain amplitude is in line with standard literature behaviors. Therefore, the numerical model in the present paper can be used to simulate the dynamic properties of clay.

The site soil is simulated by the quadUP element. The soft soil constitutive calculation parameters are obtained by referring to the recommended values of OpenSEES clay constitution, specifically as listed in Table 1 [29]. The designed strength of the concrete with established embedded depth is C40 and the density is 2500 kg/m^3 [30, 31]. The adoption of the fiber section unit of the underground structure considers its nonlinear dynamic performance. The schematic diagram of the fiber section is shown in Figure 5 [32]. Specifically, the Concrete02 constitutive model (modified Kent–Park concrete model) is used in the structural concrete, and the stress-strain relationship is shown in Figure 6(a). The steel bar uses Steel02 dynamic isotropic hardening bilinear material model, and the stress-strain relation is shown in Figure 6(b), in which the elastic modulus of the steel bar is 200 GPa and the yield strength is 400 MPa.

The north-south component of the 1995 Kobe earthquake is scaled 0.2 g and used as the horizontal excitation in the analyses. The magnitude is 6.9. North-south component was recorded at the Kobe Japanese Meteorological Agency (JMA) station during the Hyogo-ken Nanbu (Kobe) earthquake (Rjb (km): 0.94, Rrup (km): 0.96, and VS30 (m/s): 312). The Kobe seismic wave with duration of 30 s is selected and input horizontally from the base rigid boundary, and the acceleration input of the seismic ground motion and corresponding Fourier spectrum are shown as Figure 7. Initial ground stress balance (the elastic + plastic stage) is first carried out, and then the seismic action is applied. The numerical calculation is completed by a 64-bit 32-core CPU-64G memory DELLT7600 high-performance desktop workstation, and all the numerical results are extracted and visualized by the self-compiled MATLAB interface program.

3. Analysis of Seismic Response of Burial Depth to the Subway Station Structure in Saturated Soft Foundation

3.1. Influence of Burial Depth on Displacement of the Subway Station Structure. Figure 8 shows the residual displacement

Table 1: Model parameters of soft clay.

Soil parameter	ρ (kg/m^3)	G_{ref} (MPa)	B_{ref} (MPa)	c (kPa)	γ_{max}	φ	n_p
Parameter value	1700	17	79	18	0.1	0	0

Note: ρ is the saturated soil mass density; G_{ref} is the reference low-strain shear modulus; B_{ref} is the reference bulk modulus; c is the apparent cohesion at zero effective confinement; γ_{max} is an octahedral shear strain at which the maximum shear strength is reached; φ is the friction angle at peak shear strength in degrees; n_p is an optional nonnegative constant defining variations of G and B as a function of initial effective confinement.

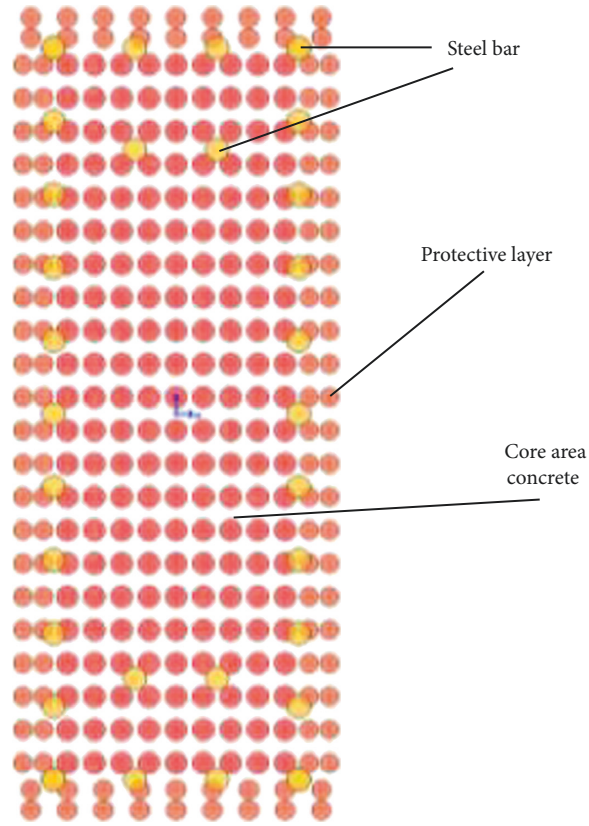

Figure 5: Schematics of fiber cross section.

of the soft site after the earthquake under different burial depth conditions. It can be seen from Figure 8 that, with the increase of burial depth, the uneven uplift effect of the subway station structure caused by the movement and extrusion of soil from the far field to the bottom of the floor is weakened gradually. The displacement time history curve of the middle point of the floor of the subway station structure in the soft soil site under different burial depth conditions is shown in Figure 9. It can be seen from Figure 9 that the peak of the horizontal and vertical displacements time history curve of the subway station structure gradually decreases with the increase of the burial depth, and the uplift amount of the typical point of the structure of 11 m (burial depth) is reduced by 50% than that of 5 m (with burial depth). It can be seen that the burial depth of the subway station structure in the saturated soft soil site has a significant influence on the uneven uplift effect.

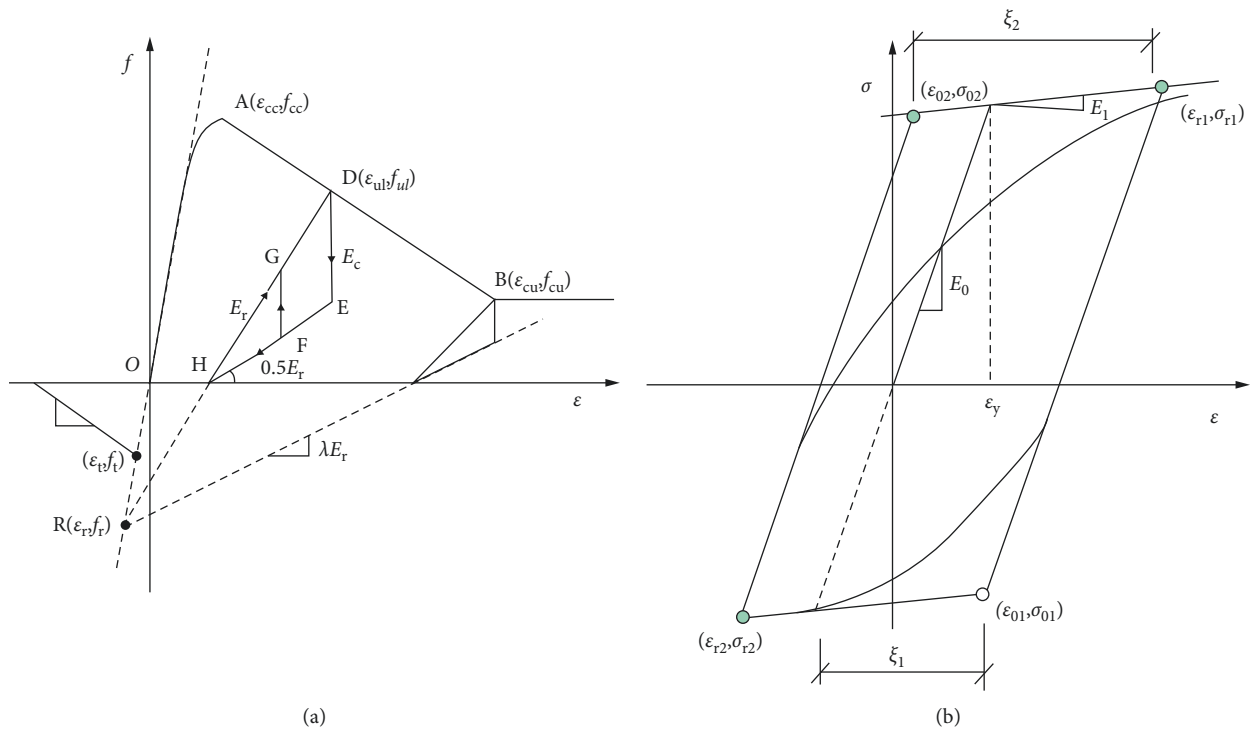

Figure 6: Constitutive model of reinforced concrete: (a) stress-strain curve of concrete; (b) stress-strain curve of the steel bar.

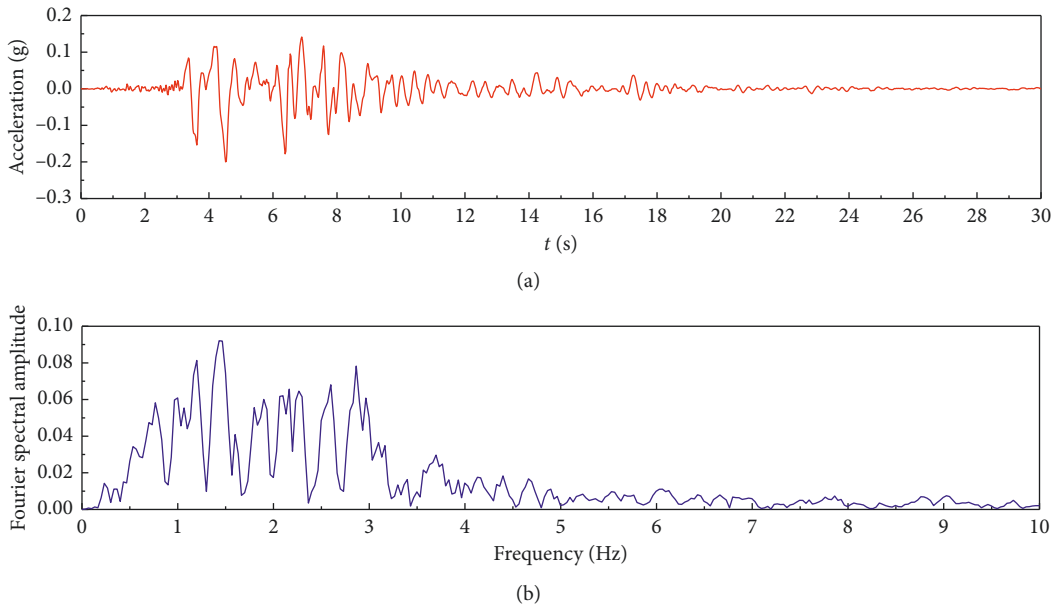

Figure 7: Ground motion acceleration input: (a) ground motion time history; (b) Fourier spectrum.

3.2. Influence of Burial Depth on the Peak of Soil Dynamic Pore Pressure Ratio. According to the principle of effective stress, the dynamic pore pressure ratio (representative symbol: DPPR) is computed as the ratio of excess pore pressure to initial effective vertical stress. Figure 10 shows the peak envelope diagram of the dynamic pore pressure ratio of the soft soil site under different burial depth conditions. It can be seen from the diagram that the predominance area of the dynamic pore pressure ratio peak of the soft soil around the shallow-buried subway station shows a typical ring-shaped distribution characteristic, and the maximum dynamic pore pressure ratio (0.5) appears near the floor of the subway station and the shear wall. With the increase of the burial depth of the station structure, the vertical effective stress level of the deep soil near the structure becomes higher, and the inertial dynamic extrusion effect of the overlaying soil in the station structure is increased accordingly. Therefore, the range of the dynamic pore pressure ratio peak area of soft

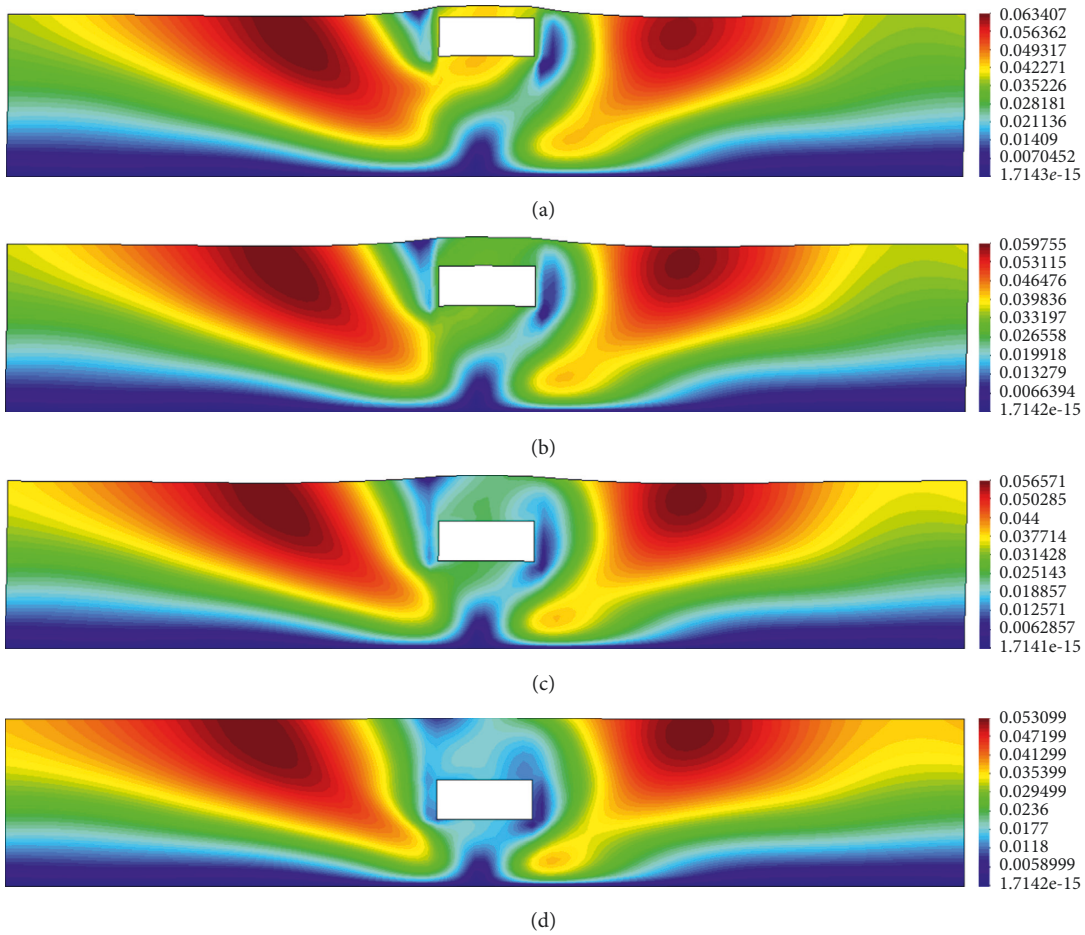

Figure 8: Contours of postearthquake residual displacement of soft soil ground with different burial depths (unit: (m): (a) 2 m; (b) 5 m; (c) 8 m; (d) 11 m.

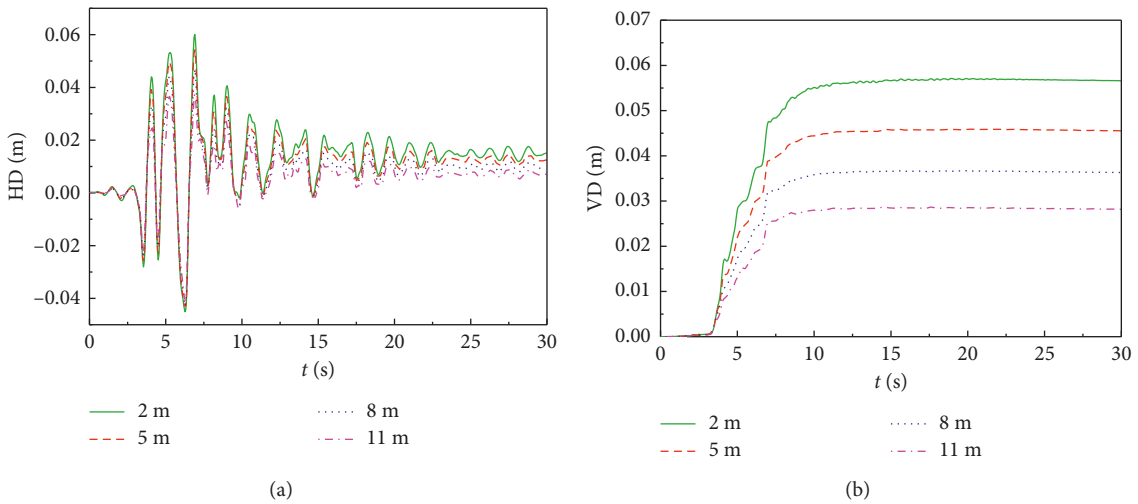

Figure 9: Time history of displacement of subway station structures with different burial depths: (a) horizontal displacement; (b) vertical displacement.

soil around the subway station structure is gradually close to the structure from outside, and the peak also decreases.

Figure 11 shows the time-history curves of the dynamic pore pressure ratio at the locations of characteristics points of soft soil sites under different burial depth conditions. It can be seen from Figure 11 that, with the increase of the burial depth of the station structure, the dynamic pore pressure ratio peak of the soil typical points F_1 and F_2 around

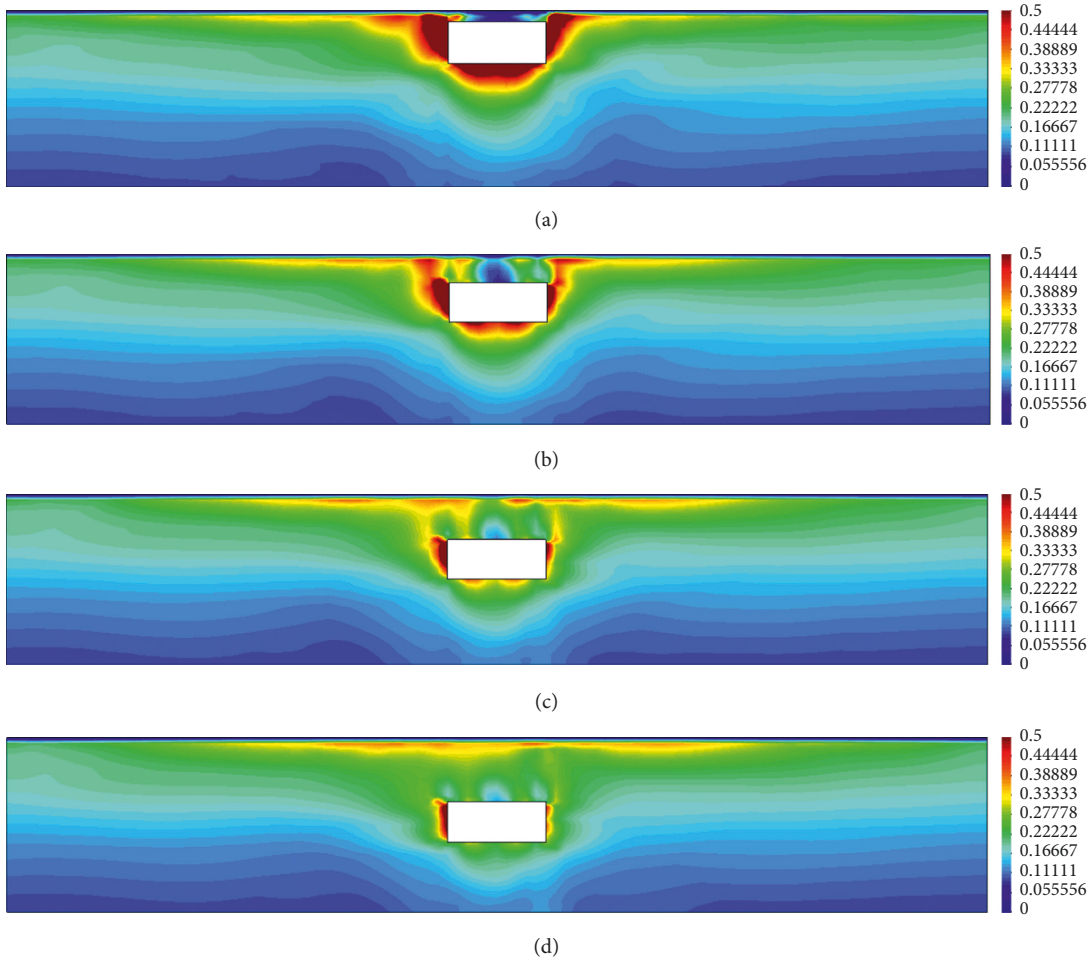

Figure 10: Contours of peak response of the dynamic pore pressure ratio of soft soil ground with different burial depths: (a) 2 m; (b) 5 m; (c) 8 m; (d) 11 m.

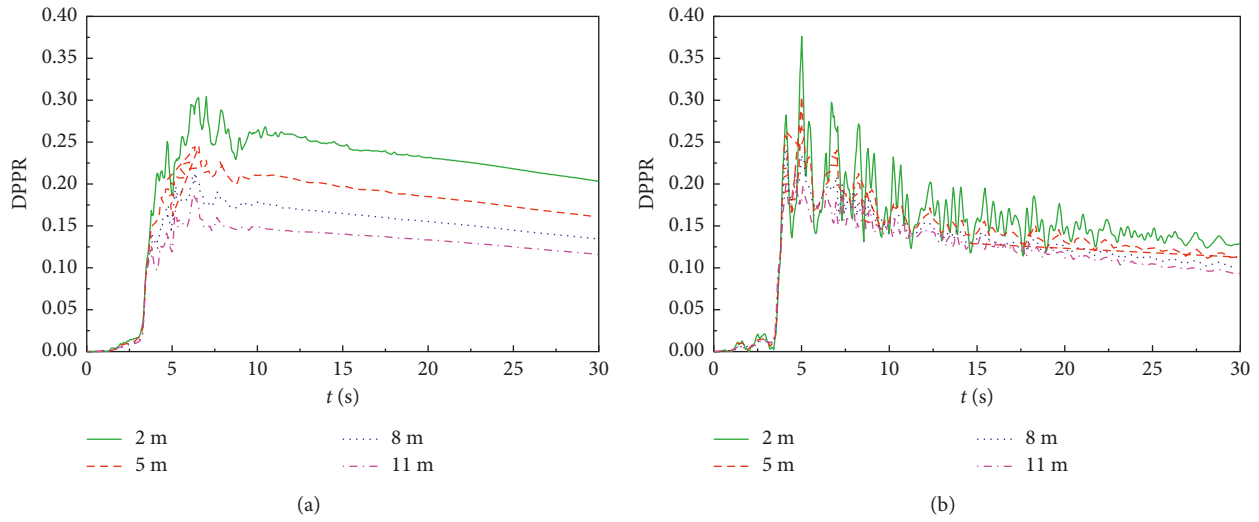

Figure 11: Time-history curves of the dynamic pore pressure ratio of typical points with different burial depths in soft soil ground: (a) F_1; (b) F_2.

the structure gradually decreases, which is in accordance with the variation of the peak range and peak level of the dynamic pore pressure ratio of the soft soil around the subway station structure in Figure 9.

3.3. Influence of Burial Depth on Internal Force Response of the Subway Station Structure. The position of the structural column-slab joint as shown in Figure 12 is selected as the typical section of the structure for analysis. For example, Tables 2–4 show the peak of the internal force response at the typical section of the subway station structure under different burial depth conditions, and the figure in the brackets in the tables is the peak increase percentage of the dynamic internal force with the burial depth of 11 m compared with that of 2 m. It can be seen from the tables that, with the increase of burial depth, the peak position of the maximum internal force in the whole structure will also be adjusted under the seismic action. Specifically, the maximum axis force peak of the whole structure appears at the left end of the floor (position of P_1) when the burial depth is 2 m, while the maximum axial peak position of the whole structure appears at the lower end of the middle column (position of P_7) when the burial depth is 11 m; the maximum shear peak of the structure appears at the lower end of the left wall (position of P_5) when the burial depth is 2 m, and when the burial depth is 11 m, the maximum shear peak position of the whole structure appears at the lower end of the right wall (position of P_9); and the maximum bending moment peak of the whole structure under the condition that the burial depth is 2 m appears at the left end of the floor (position of P_1), while the maximum bending moment peak position of the overall structure appears at the middle end of the roof (position of P_{12}) when the burial depth is 11 m. In addition, with the increase of burial depth, the peak of internal forces at typical sections of structural members also increases in varying degrees. In particular, for the typical section of the same structure, the maximum bending moment peak of the middle end (position of P_2 and P_3) of the structure floor when the burial depth is 11 m has an increase rate of about 750% compared with that of 2 m (burial depth), which is far greater than the increase rate of the maximum internal force peak of the other typical sections in the whole structure.

The above analysis is aimed at the maximum internal force peak of the key point of the structure and the increase with the change of the burial depth. In order to further understand the effect of different burial depth conditions on the dynamic internal force response of the structure under the seismic action, the nondimensional dynamic response evaluation index R is defined, which is the ratio of additional dynamic internal force to total internal force (seismic action + gravity action) caused by seismic action.

Figure 13 shows the R distribution of the dynamic evaluation index at the typical section of the structure when the burial depth is 2 m. According to the order of the value of R in each dynamic internal force evaluation index in the figure, the positions of the first 2 typical sections are selected as the most unfavorable antiseismic component position in the subsequent analysis. Specifically, the dynamic axial force and dynamic bending moment of P_{14}, the dynamic shear and dynamic bending moment of P_{10}, the dynamic axial force of P_{11}, and the dynamic shear force of P_6 are selected as the most unfavorable antiseismic component positions and indexes, and the change of corresponding dynamic evaluation indexes with burial depth is analyzed.

Figure 14 shows that the dynamic evaluation index of the most unfavorable typical section above varies with the burial depth of the structure. It can be seen from Figure 14 that, with the increase of the structural burial depth, the value of the dynamic response evaluation index R for each corresponding position has a decreasing trend, which illustrates from the other perspective that the dynamic failure of the shallow-buried subway station in the saturated soft soil site may be more serious. In fact, the internal force increase of the underground structure caused by the gravity of the system is larger than that of the additional internal force, that is, the R ratio decreases. The dynamic evaluation index of the dynamic bending moment at the upper end of the right wall (position of P_{10}) and the right end of the roof (position of P_{14}) is the highest, and the changes with the burial depth of the structure are also the most significant.

In particular, the shear and bending moment of the middle column are close to zero only under the gravity, there is $R \longrightarrow 1$ at each burial depth condition for the middle column, and the nondimensional dynamic response evaluation index R is not applicable. In particular, the increase of the shear and bending moment of the middle column is close to zero only under the system gravity; that is, for the middle column, there is $R \longrightarrow 1$ at each burial depth condition, and the nondimensional dynamic response evaluation index R is not applicable. As we know, the roof collapse caused by dynamic failure of the middle column is one of the important forms of seismic damage of the subway station structure. On this basis, in addition to the analysis of the most unfavorable seismic position according to the R value increase, the middle column is further selected as the most unfavorable seismic component position, and the change of additional dynamic internal force which increases with the burial depth is adopted for evaluation and analysis. Figure 14 shows that the additional internal forces of the upper and the lower ends of the middle column vary with the burial depth. As shown in Figure 15, the additional dynamic shear and dynamic bending moment at the upper end of the middle column (position of P_8) are most significantly influenced by the burial depth (the variation coefficients are 0.468 and 0.464, resp.), second to which is the additional dynamic shear and the dynamic bending moment at the lower end of the middle column (position of P_7) (the variation coefficients are 0.445 and 0.448, resp.), and the additional dynamic axial force of the upper and lower ends of the middle column are most slightly influenced by the burial depth (the variation coefficient is 0.199). In addition, Tables 2–4 also show that the maximum internal force peak and the change and increase of the middle column are lower than those of the other key characteristic positions under all burial depth conditions.

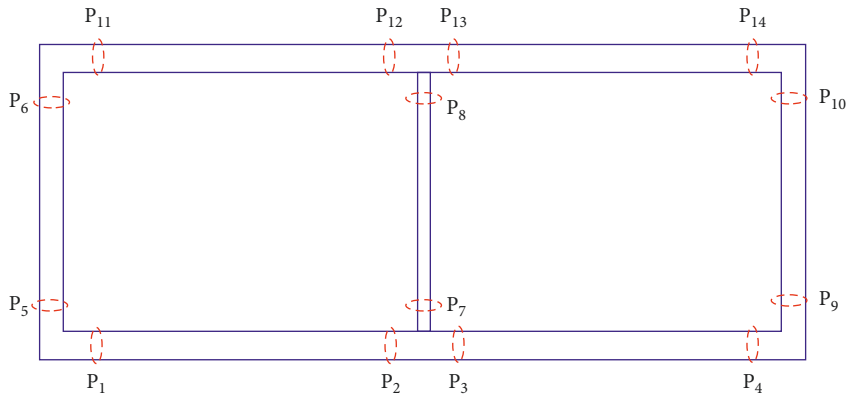

Figure 12: Schematic diagram of key parts of dynamic force of the subway station structure.

Table 2: The maximum axial forces at typical sections of the structure with different burial depths (unit: kN).

Burial depth (m)	P_{11}	P_{12}	P_{13}	P_{14}	P_6	P_8	P_{10}
2 m	550	544	526	598	768	2201	783
5 m	1331	1342	1317	1382	1636	3778	1648
8 m	2028	2045	2009	2095	2454	5427	2484
11 m	2686 (↑388%)	2661 (↑**389%**)	2606 (↑395%)	2761 (↑362%)	3239 (↑322%)	7080 (↑**222%**)	3281 (↑319%)
Burial depth (m)	P_1	P_2	P_3	P_4	P_5	P_7	P_9
2 m	2335	2200	2196	2332	1512	2269	1499
5 m	2880	2709	2709	2869	2362	3848	2320
8 m	3348	3116	3144	3314	3216	5495	3114
11 m	3844 (↑65%)	3568 (↑62%)	3583 (↑63%)	3843 (↑65%)	4174 (↑176%)	7150 (↑**215%**)	3889 (↑159%)

Table 3: The maximum shear forces of typical sections of the structure with different burial depths (unit: kN).

Burial depth (m)	Position of P_{11}	Position of P_{12}	Position of P_{13}	Position of P_{14}	Position of P_6	Position of P_8	Position of P_{10}
2 m	467	1043	1032	466	580	39	618
5 m	1135	1701	1681	1168	1239	69	1289
8 m	1837	2416	2341	1875	1882	102	1966
11 m	2459 (↑427%)	3131 (↑200%)	2994 (↑190%)	2488 (↑**434%**)	2501 (↑331%)	131 (↑**236%**)	2597 (↑320%)
Burial depth (m)	P_1	P_2	P_3	P_4	P_5	P_7	P_9
2 m	1482	834	846	1474	1795	53	1780
5 m	2053	1502	1539	2043	2349	77	2270
8 m	2524	2219	2257	2569	2762	116	2740
11 m	3015 (↑103%)	2940 (↑253%)	2947 (↑248%)	3071 (↑108%)	3157 (↑76%)	144 (↑**172%**)	3200 (↑80%)

Table 4: The maximum bending moments at typical sections of the structure with different burial depths (unit: kN·m).

Burial depth (m)	P_{11}	P_{12}	P_{13}	P_{14}	P_6	P_8	P_{10}
2 m	608	2710	2709	631	608	143	631
5 m	1839	3739	3737	2034	1839	248	2034
8 m	3138	4935	4836	3441	3137	367	3441
11 m	4286 (↑605%)	6019 (↑122%)	5852 (↑116%)	4590 (↑627%)	4284 (↑605%)	472 (↑**230%**)	4589 (↑627%)
Burial depth (m)	P_1	P_2	P_3	P_4	P_5	P_7	P_9
2 m	3228	443	445	3169	3225	156	3165
5 m	4232	1493	1496	4118	4230	256	4106
8 m	5066	2608	2645	4913	4993	385	4895
11 m	5741 (↑78%)	3754 (↑747%)	3823 (↑**759%**)	5747 (↑81%)	5699 (↑77%)	482 (↑**209%**)	5701 (↑80%)

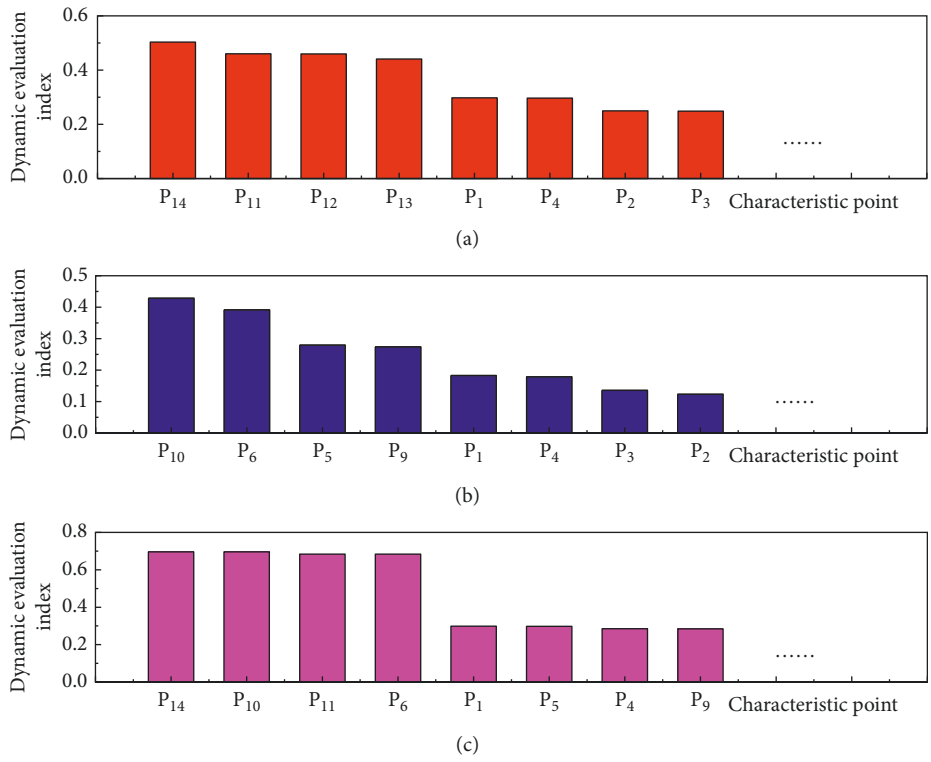

Figure 13: Comparison of the dynamic index at typical sections of the structure with 2 m burial depth.

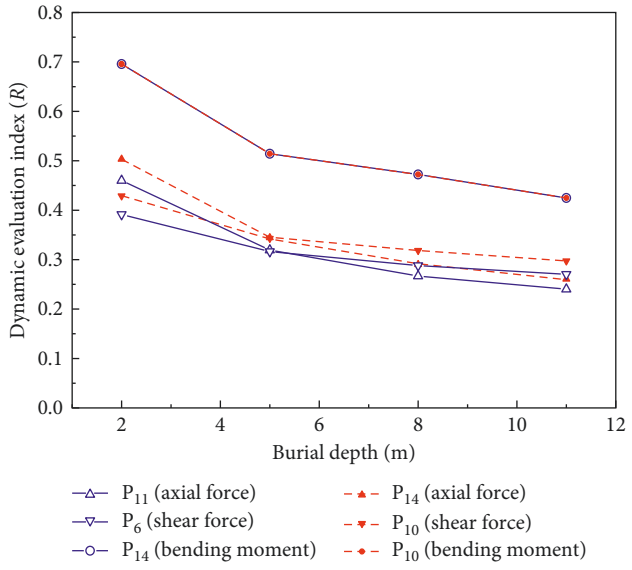

Figure 14: Variations of the dynamic index with burial depths at typical sections.

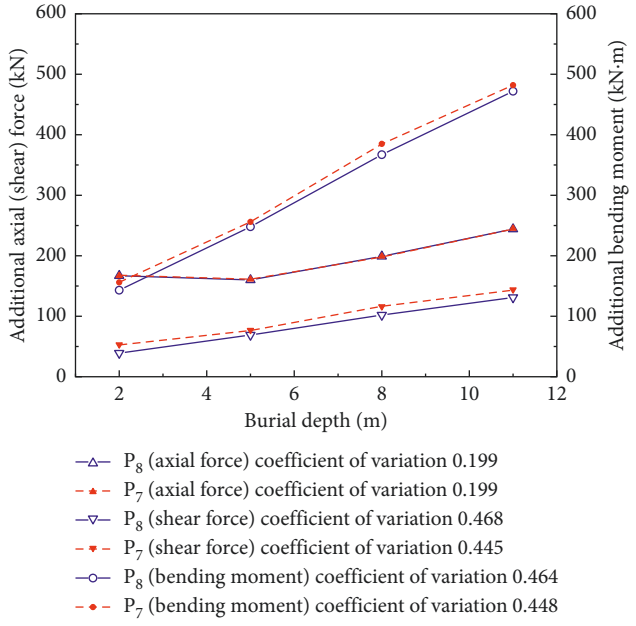

Figure 15: Variations of dynamic internal forces with burial depths at typical sections.

4. Conclusions

Based on the *u-p* form of Biot's dynamic consolidation equation and the effective stress dynamic solution method of saturated two-phase medium, a numerical model of effective stress coupled dynamic analysis for the saturated soft soil site-subway station structure interaction system is established in the present paper, and the seismic dynamic response law of the saturated soft soil site-subway station structure interaction system under different burial depth conditions is analyzed. The calculation and analysis results show the following:

(1) With the increase of burial depth of the station, the uneven uplift effect of the subway station structure caused by the movement and extrusion of soil from the far field to the bottom of the floor is weakened

gradually, and the burial depth in the saturated soft soil site has a significant influence on the uneven uplift effect.

(2) With the increase of the burial depth of the station structure, the soil's vertical effective stress level at the depth of the structure becomes higher, and the inertial dynamic extrusion effect of the overlying soil layer is enhanced simultaneously. The range of the dynamic pore pressure ratio peak of the soft soil around the station structure is gradually close to the structure from the outside, and the peak level also decreases.

(3) With the increase of the burial depth of the station structure, the value of nondimensional dynamic response evaluation index R for all positions shows a decreasing trend, in which the dynamic moment evaluation index of the upper end of the right wall and the right end of the roof is the largest, and the change with the structural burial depth is the most significant.

(4) For the internal force index of the middle column, the additional dynamic shear and dynamic bending moment at the upper end of the middle column are most significantly affected by the burial depth of the structure, followed by the lower end of the middle column. Compared with the corresponding value of the other key characteristic positions of the structure, the maximum internal force peak of the middle column and the increase with the burial depth are lower.

Data Availability

The data used to support the findings of this study are available from the corresponding author upon request.

Conflicts of Interest

The authors declare that there are no conflicts of interest regarding the publication of this paper.

Acknowledgments

This research was supported by the National Natural Science Foundation of China (Grant no. 51578100), the Funding on Fundamental Research in Central Universities (Grant nos. 3132014326 and 3132017022), the Open Funding of Key Laboratory of Ministry of Education for Geomechanics and Embankment Engineering, Hohai University (Grant no. 20161018), and the Key Laboratory Program of Ministry of Education for Urban Security and Disaster Engineering, Beijing University of Technology (Grant no. 201501).

References

[1] K. Kawashima, "Seismic design of underground structures in soft ground–a review," in *Geotechnical Aspects of Underground Construction in Soft Ground*, O. Kusakabe, K. Fujita, and Y. Miyazaki, Eds., Balkema, Rotterdam, 1999.

[2] Y. M. A. Hashash, J. J. Hook, B. Schmidt et al., "Seismic design and analysis of underground structures," *Tunnelling & Underground Space Technology*, vol. 16, no. 4, pp. 247–293, 2001.

[3] K. Pitilakis and G. Tsinidis, "Performance and seismic design of underground structures," in *Earthquake Geotechnical Engineering Design, Geotechnical Geological and Earthquake Engineering*, M. Maugeri and C. Soccodato, Eds., vol. 28, pp. 279–340, Springer, Geneva, Switzerland, 2014.

[4] G. X. Chen, S. Chen, X. L. Du et al., "Review of seismic damage, model test, available design and analysis methods of urban underground structures: retrospect and prospect," *Journal of Disaster Prevention and Mitigation Engineering*, vol. 36, no. 1, pp. 1–23, 2016, in Chinese.

[5] C. M. S. John and T. F. Zahrah, "Aseismic design of underground structures," *Tunnelling & Underground Space Technology*, vol. 2, no. 2, pp. 165–197, 1987.

[6] N. Yoshida, "Underground and buried structure," in *Earthquake Geotechnical Engineering*, Sêco e Pinto, Ed., vol. 3, pp. 987–992, Balkema, Rotterdam, Netherlands, 1999.

[7] W. Z. Chen, W. P. Song, W. S. Zhao et al., "Research progress of seismic analysis methods and performance evaluation in underground engineering," *Chinese Journal of Rock Mechanics and Engineering*, vol. 36, no. 2, pp. 310–325, 2017, in Chinese.

[8] X. L. Du, Y. Li, C. S. Xu et al., "Review on damage causes and disaster mechanism of Daikai subway station during 1995 Osaka-Kobe Earthquake," *Chinese Journal of Geotechnical Engineering*, vol. 40, no. 2, pp. 223–236, 2018, in Chinese.

[9] H. B. Liu and E. X. Song, "Effects of burial depth on the liquefaction response of underground structures during an earthquake excitation," *Journal of Tsinghua University (Science&Technology)*, vol. 45, no. 3, pp. 301–305, 2005, in Chinese.

[10] H. B. Liu and E. X. Song, "Seismic response of large underground structures in liquefiable soils subjected to horizontal and vertical earthquake excitations," *Computers and Geotechnics*, vol. 32, no. 4, pp. 223–244, 2005, in Chinese.

[11] E. Bilotta, G. Lanzano, G. Russo et al., "Methods for the seismic analysis of transverse section of circular tunnels in soft ground," in *Proceedings of aISSMGE-ERTC12 Workshop at XIV ECSMGE Geotechnical Aspects of Ec8*, Patron Editore, Bamenda, Cameroon, January 2007.

[12] J. Y. Chen, R. Z. Wen, P. Q. Yu et al., "Numerical analysis of seismic response of a shallow-buried subway station structure in soft soil," *World Earthquake Engineering*, vol. 25, no. 2, pp. 46–53, 2009, in Chinese.

[13] H. Y. Zhuang, X. X. Wang, and G. X. Chen, "Earthquake responses of subway station with different depths of soft soil," *Chinese Journal of Geotechnical Engineering*, vol. 31, no. 8, pp. 1258–1266, 2009, in Chinese.

[14] A. Amorosi and D. Boldini, "Numerical modelling of the transverse dynamic behavior of circular tunnels in clayey soils," *Soil Dynamics & Earthquake Engineering*, vol. 29, no. 6, pp. 1059–1072, 2009.

[15] C. H. Chen, T. T. Wang, F. S. Jeng et al., "Mechanisms causing seismic damage of tunnels at different depths," *Tunnelling & Underground Space Technology*, vol. 28, no. 1, pp. 31–40, 2012.

[16] S. Wang, D. C. Lu, and X. L. Du, "Research on underground structure seismic damage using static-dynamic coupling simulation method," *Rock and Soil Mechanics*, vol. 33, no. 11, pp. 3483–3488, 2012, in Chinese.

[17] P. H. Li and C. Z. Qi, "Effect of different soil layer distribution on seismic response of underground structure in layered foundation," *Journal of PLA University of Science and Technology (Natural Science Edition)*, vol. 15, no. 5, pp. 457–461, 2014, in Chinese.

[18] G. Tsinidis, "Response characteristics of rectangular tunnels in soft soil subjected to transversal ground shaking," *Tunnelling and Underground Space Technology*, vol. 62, no. 1, pp. 1–22, 2017.

[19] C. Y. Cui, X. L. Cheng, Z. G. Sun et al., "Analyses of seismic response and parametric sensitivity of subway station surrounded by saturated soft soil," *Journal of Railway Engineering Society*, vol. 34, no. 3, pp. 92–98, 2017, in Chinese.

[20] Y. Di and X. W. Tang, "Numerical simulation for large deformation dynamic problem in two-phase media," *Engineering Mechanics*, vol. 24, no. 12, pp. 47–52, 2007, in Chinese.

[21] M. T. Luan, X. L. Zhang, Q. Yang et al., "Numerical analysis of liquefaction of porous seabed around pipeline fixed in space under seismic loading," *Soil Dynamics and Earthquake Engineering*, vol. 29, no. 5, pp. 855–864, 2009.

[22] A. Ghassemi, A. Pak, and H. Shahir, "Numerical study of the coupled hydro-mechanical effects in dynamic compaction of saturated granular soils," *Computers and Geotechnics*, vol. 37, no. 1-2, pp. 10–24, 2010.

[23] Y. Zou, "*Study on seismic response laws and seismic design methods of underground structures*," Ph.D. thesis, Institute of Engineering Mechanics, China Earthquake Administration, Harbin, China, 2015.

[24] G. D. Hatzigeorgiou and D. E. Beskos, ""Soil–structure interaction effects on seismic inelastic analysis of 3-D tunnels," *Soil Dynamics & Earthquake Engineering*, vol. 30, no. 9, pp. 851–861, 2010.

[25] H. Sedarat, A. Kozak, Y. M. A. Hashash et al., "Contact interface in seismic analysis of circular tunnels," *Tunnelling & Underground Space Technology*, vol. 24, no. 4, pp. 482–490, 2009.

[26] D. D. Zhao, "*Experimental study and numerical simulation on seismic response of urban underground subway structures*," Ph.D. thesis, Tsinghua University, Beijing, China, 2013.

[27] A. C. Chan and A. Elgamal, "Nonlinear modeling of large-scale ground-foundation-structure seismic response," *Journal of Earthquake Technology*, vol. 44, no. 2, pp. 325–339, 2007.

[28] M. Vucetic and R. Dobry, "Effect of soil plasticity on cyclic response," *Journal of Geotechnical Engineering*, vol. 117, no. 1, pp. 89–107, 1991.

[29] F. Mckenna, S. Mazzoni, M. H. Scott et al., *Opensees Command Language Manual S. l.*Pacific Earthquake Engineering Research Center, Berkeley, CA, USA, 2006.

[30] G. Wang, J. M. Zhang, and X. Wei, "Seismic response analysis of a subway station in liquefiable soil," *Chinese Journal of Geotechnical Engineering*, vol. 33, no. 10, pp. 1623–1627, 2011, in Chinese.

[31] X. L. Du, G. Wang, and D. C. Lu, "Earthquake damage mechanism analysis of Dakai Metro Station by Kobe Earthquake," *Journal of Disaster Prevention and Mitigation Engineering*, vol. 36, no. 2, pp. 165–171, 2016, in Chinese.

[32] Y. Gu, S. M. Zhuang, W. D. Zhou et al., "Analysis of nonlinear seismic response of subway station considering saturated soil," *Rock and Soil Mechanics*, vol. 36, no. 11, pp. 3243–3251, 2015, in Chinese.